Chapter 5: Classifying remotely sensed environmental metrics

5. 1 Introduction

The objective of this chapter was to create a land cover dataset for the study site where the classes would be selected based on the potential associations between population or development and the environment that were found in the literature and during field observations.

Remotely sensed satellite images can be used to obtain information about environmental conditions across large spatial areas of the Earth (Lillesand et al. 2004). Land features such as grass, concrete, water, woodland and agriculture reflect electromagnetic radiation in different ways and have specific spectral patterns (Campbell 2002). These different patterns enable remote sensors to distinguish between different types of land covers. There are two overlapping types of classification that can be performed using remotely sensed images, (i) land cover mapping and (ii) land use mapping. Land cover maps classify information on the type of feature present on the Earth's surface. Land use maps classify information on the "human activity or economic function associated with a specific piece of land" (Lillesand et al. 2004 p.215). For operational purposes it is often necessary to develop classification schemes that combine land use and land cover classes. This can result in the need to split spectrally similar classes. For example, Koch et al. (2007) found that agricultural practices in Paraguay could be split into two distinct types; (i) large scale commercial farms, and; (ii) small scale production by small land holders. Spectrally the differences between the two types of agriculture were very small. However, using spatial and textural information contained within the scene it was possible to distinguish between the two quite clearly.

5.1.1 Using Landsat for land cover classification

The Landsat programme provides a large historical and largely uninterrupted Earth observation data set dating back to 1972. The current satellite and that used for analysis in this research is Landsat 7 Enhanced Thematic Mapper Plus (ETM+) with a 30 m spatial resolution (Irons 2010).

There are important differences between detection and identification of land cover classes (Millette et al. 1995). Detection only requires a change in contrast between a group of pixels and the background, whereas, identification requires each feature to have a unique spectral signature for it to be computationally distinguished from other classes. Thus, land features with similar spectral properties may be easily detected but more difficult to identify using spectral information in a satellite sensor image (Blaschke et al. 2005). The data from Landsat ETM+ can be used to map land cover classes however, the potential for mapping land uses is limited due to the spatial resolution of the sensor. Anderson et al. (1976) suggested that nine classes could be classified using 30 m spatial resolution imagery. This is because, for example, the 30 m resolution imagery is not able to identify different types of agricultural crops (Millette et al. 1995). However, spatial information contained within the remotely sensed image can be used in conjunction with the spectral information to classify land features with similar spectral properties.

5.1.2 Object-based land classification

Often, to distinguish between different land cover classes, the value and texture of surrounding pixels can be used (Aplin and Smith 2008; Blaschke and Strobl 2001; Flanders et al. 2003). Unlike per-pixel classification methods object-based approaches to image analysis allow the use of spectral and spatial information contained within an image to be used in the classification process (Blaschke and Strobl 2000; Flanders et al. 2003).

To make use of the textural and spatial data available in remotely sensed imagery object-based analysis uses image segmentation prior to classification which groups pixels with similar attributes together into homogenous objects. This is conducted by first considering each pixel as a separate object and merging similar objects using localised homogeneity thresholds. Once

the homogeneity threshold is exceeded the merging process ends and an object boundary is defined (Darwish et al. 2003). When attempting to split spectrally similar but spatially distinct classes in classification procedures object-based analysis can be more accurate than pixel based methods. For example, results in Koch et al. (2007) showed that an object-based approach had an overall accuracy of 84% compared to 43% for maximum-likelihood per-pixel classifier.

For operational purposes the classification of Landsat ETM+ data for Assam merged land cover and land use classes. Several of these classes were spectrally very similar but could be identified using a combination of spatial and textural information. Therefore, object-based land use/land cover classification methods were used.

5.2 The problem of cloud in land cover classification using Landsat data

Estimates suggest that cirrus cloud covers up to 30% of the Earth's surface at any time (Wylie and Menzel 1999) and this can rise to more than 50% in tropical and sub-tropical locations (Chepfer et al. 2000) where cirrus cloud can persist for extensive periods (Comstock et al. 2002). The low optical depth of cirrus clouds can cause problems for land cover classification (Dessler and Yang, 2003) because pixels often contain a mixture of atmospheric cloud and land signals. Unlike cumulus cloud, cirrus cloud is partially transparent and, thereby, difficult to remove entirely. However, left in place, cirrus cloud can be problematic for studies utilising remotely sensed satellite sensor imagery for further analysis because pixels that are cloud covered may be incorrectly assigned to a land cover class with similar spectral and thermal properties to clouds rather than to the true underlying land cover class.

The Landsat ETM+ sensor lacks wavebands that are able to detect cirrus clouds which, by contrast, are available on other satellite sensors such as the Moderate Resolution Imaging Spectroradiometer (MODIS) (Gao et al. 2002). The presence of these bands enables more accurate cloud masks to be developed (Platnick et al. 2003). Thus, cirrus cloud cover is a problem when using Landsat ETM+ data. Irish et al. (2006) highlighted that "...the ETM+ spectral bands do not easily detect semi-transparent clouds such as Cirrus Uncinus...Cirrus

Fibratus and cloud edges" (p.1180). If an image on a specific date is required for subsequent data analysis there may be no option but to select cloud affected imagery and find a method to identify and mask this cloud (El-Araby et al. 2005). Therefore, although the data cost constraint for regional studies has been removed for Landsat data their use may be hampered by a lack of simple to implement cirrus cloud removal procedures.

Initial analysis of the Landsat ETM+ images available for Assam revealed substantial amounts of cloud (Table 5.1). Transparent clouds were a particular problem in Assam as they were found to have very similar spectral properties to several intended classes. For example, shallow water pixels with sand and silt had similar properties to areas of bare land with cloud coverage. Wet bare land also had similar spectra to transparent clouds. Often remotely sensed images with such cloud cover issues would not be considered for analysis (Foody 2002: Wen et al. 2001). Operational reasons such as the need to have satellite data near to the time of the 2001 Indian census enumeration meant these images were the most suitable for subsequent analysis. The presence of cloud and transparent cloud would potentially result in significant limitations for the environmental data to be used in subsequent analysis. Therefore, before image classification was conducted, cloud coverage was identified and removed.

Table 5.1 Cloud percentages for Landsat scenes covering Assam in 2001[14].

Scene (Path/Row)	Feb	Mar	Apr	May	Jun	Jul	Aug	Sep	Oct	Nov	Dec
134/041	8	95		85	82	58	62	83	0		1
135/041	9	37	90	99	32	95	79	33	17		11
135/042		10	38	80	94	98	88	87	83	No Data Available	1
136/041	13	57	51	9			100	98	6		1
136/042	0	24	38	15		88	100	94	7		37
137/041		32	47		96	56	71	87	4		7

5.2.1 Identifying and masking cloud in Landsat Data

Several cloud identification and masking techniques have been proposed for Landsat data. Helmer and Reufenacht (2005) created cloud and cloud shadow masks for Landsat Thematic Mapper (TM) imagery using the Iterative Self-organising data analysis (ISODATA) technique and manual editing. Results were variable with 73% to 87% overall accuracy for images from 2000, but 18% to 92% in 1991.

To increase discrimination between low altitude cloud and ground features with similar spectral properties such as rooftops Melesse and Jordan (2002) augmented the data to be used in ISODATA with the Landsat TM thermal band. Data were also augmented using the normalized difference vegetation index (NDVI) to increase discrimination between low altitude cloud and ground features with small amounts of vegetation cover. Masks created using ISODATA with

[14] Source: GloVis website metadata files http://glovis.usgs.gov/

augmented data contributed to a 2.5% increase in accuracy compared to a fuzzy classifier. It was concluded that the additional work required could not be justified for such a small increase in accuracy. However, any increase in the accuracy of a cloud mask will result in increased accuracies if data are required for further analysis. Unsupervised classifiers such as ISODATA are suitable when scenes have several very distinct classes. Optically thin cirrus clouds and cloud edges often allow some form of spectral information from the ground below to be transmitted (Wang et al. 1999). Therefore, particular ground features with similar spectral properties to transparent cloud may have higher numbers of pixels incorrectly assigned to them. Using such classification methods may, therefore, increase inaccuracies when using the images for further analysis.

Several studies have created cloud masks using supervised methods of classification that depend on defining thresholds in specific bands. Song and Civco (2002) used brightness thresholds for Landsat TM band 1 and band 4. Martinuzzi et al. (2007) used Landsat ETM+ band 1 and band 6.1 (low gain thermal band). Wang et al. (1999) used TM band 1 and band 5. Thresholds were used in different ways to identify cloud and cloud shadows. For example, Song and Civco (2002) compared the brightness in a main image (used for further analysis) with a reference image to create a brightness difference image. Band thresholds and brightness differences were then used to create cloud masks. Wang et al. (1999) used multi-image compositing or fusion for cloud masking. Cloud masks were created using absolute brightness differences between the main image and a reference image. The largest differences were said to be more likely to represent cloud. There were omission errors with this method where cloud was present in both the main and reference image.

To identify cloud edges or thinner clouds Song and Civco (2002) and Martinuzzi et al. (2007) used tolerance thresholds to extend the thresholds. A Digital Number (DN) tolerance threshold of 10 was employed by Song and Civco (2002) whereas Martinuzzi et al. (2007) used a three pixel buffer around each masked cloud.

Although not designed to be used as a per-pixel cloud mask, the scene averaged automated cloud cover assessment (ACCA) algorithm identifies clouds in Landsat ETM+ imagery (Irish 2000). The method integrates brightness, temperature and composite thresholds to discriminate cloud from a range of land cover types that can have similar spectral properties to clouds such as bare sand and rock. Such a mask is created as part of the procedure and Irish et al. (2006) recommended that this mask could be made available when users download Landsat ETM+ imagery.

5.2.2 Limitations of Cloud Masking Methods

The techniques highlighted above all have limitations for creating accurate cloud masks. The main limitation for cloud mask creation using Landsat imagery is the lack of a band designed to identify cirrus clouds. Irish et al. (2006) described the clouds identified by the ACCA method "...as optically thick or nearly opaque..." (p. 1180). The series of thresholds used for the ACCA algorithm enables a hierarchical model to be built that can separate cloud, non-cloud and ambiguous pixels from a range of land covers with similar spectral and thermal responses. However, the ACCA method suffers from omission errors associated with thin cirrus clouds (Irish et al. 2006). The method also suffers from commission errors associated with low solar illumination over snow and ice (Choi and Bindschadler 2004).

Image compositing methods such as those used in Wang et al. (1999) could require unfeasibly large numbers of images to decrease commission errors and in sub-tropical and tropical locations it may not be possible to acquire imagery with acceptable levels of cloud (< 40%) during particular times of the year. DN or pixel buffer tolerance thresholds can help mask transparent cloud. However, DN thresholds will introduce commission errors by using a blanket threshold across the whole image. A pixel buffer tolerance is likely to decrease these commission errors as it adds tolerances only to areas already identified as clouds. Pixel-buffer tolerances will be affected by omission errors associated with areas of cloud not identified in the original mask.

5.2.3 Developing an Improved Method

Few cloud masking methods for Landsat imagery have been developed. Those available have been described and associated key limitations discussed. From this, it was necessary to build upon existing methods to develop an improved technique for cloud removal to ensure that cirrus clouds were captured in a mask. Consequently, this study used the Automated Cloud Cover Assessment (ACCA) method to mask cloud from images in a sub-tropical area affected by seasonal cloud. The ACCA method was adapted to increase the accuracy of identification of semi-transparent cloud using a combination of widely available pixel-based and object-based tools.

5.3 Cloud Cover Removal Method

Prior to land cover classification, cloud and transparent cloud was identified and removed from all images. First the ACCA method as presented in Irish (2000) and Irish et al. (2006) was conducted before adaptations were made to identify transparent cirrus clouds and cloud edges.

5.3.1 Automated Cloud Cover Assessment Algorithm

The ACCA algorithm combines bands two through five and seven of Landsat ETM+ data in eight filters designed to distinguish between cloud and non-cloud pixels. Irish (2000) developed a set of optimised parameters that can estimate the amount of thick and nearly opaque cloud in an image. The algorithm comprises of two passes through the data. “Pass one” identifies and removes non-cloud features from an image creating a cloud mask. It is composed of eight filters and the processing required for each filter and the reason for their use is detailed in Irish (2000) and Irish et al. (2006). “Pass two” filtering uses the temperature characteristics of clouds identified in “pass one” to identify cloud pixels missing from the “pass one” mask. However, “pass two” filtering is only performed if the desert index is greater than 0.5, the cold cloud population is over 0.4 % of the scene and the mean temperature of the cloud is less than 295K (Irish 2000).

The procedure presented in Irish (2000) was followed using ENVI 4.6 image visualisation software to generate cloud masks so that a benchmark could be set to assess any increases in accuracy from adapting the thresholds (described in Sections 5.3.2 and 5.3.3). The optical bands 1 through 5 and 7 and the low gain thermal band 6.1 were converted to absolute radiance using Equation 5.1 (see Irish 1999):

$$L_\lambda = \frac{(LMAX_\lambda - LMIN_\lambda)}{(QCALMAX - QCALMIN} * (QCAL - QCALMIN) + LMIN_\lambda \quad \text{Equation 5.1}$$

Where; *Lλ* is the spectral radiance at the sensor in watts/metre2 * ster * µm; *LMIN* and *LMAX* are the spectral radiances for each band at digital numbers 0 or 1 and 255. Thus, *LMAXλ* is the spectral radiance that is scaled to *QCALMAX* and *LMINλ* is he spectral radiance scaled to *QCALMIN* and both are in watts/metre2 * ster * µm and can be found in Irish (1999). *QCALMAX* is the maximum quantized calibrated pixel value in DN which is 255 and *QCALMIN* is the minimum quantized calibrated pixel value which is 0 for data processed before 2004. *QCAL* is the quantized calibrated pixel value in DN.

Radiance converted optical bands were then converted to Unitless Planetary Reflectance using Equation 5.2 (Irish 1999):

$$\rho_p = \frac{\pi * L_\lambda * d^2}{ESUN_\lambda * \cos\theta_s} \quad \text{Equation 5.2}$$

Where: *ρp* is the Unitless planetary reflectance; *Lλ* is the spectral radiance the sensors aperture calculated from the equation above in converting digital numbers to at sensor radiance section; *d* is the Earth-Sun distance in astronomical units based on the day of the year that the image was acquired; *ESUNλ* is the mean solar exo-atmospheric irradiances provided in Irish (1999); and θ_s is the solar zenith angle in degrees.

One of the eight “pass-one” filters is a temperature threshold as clouds are generally much colder than land. Irish (2000) used absolute temperature in Kelvin’s where pixels under 300k

were seen as potential cloud. The low gain thermal band 6.1 was converted from digital numbers (DN's) to radiance using Equation 5.1 (Irish, 1999). Equation 5.3 converts radiance into absolute Kelvin values (Irish, 1999):

$$T = \frac{K_2}{\ln\left(\frac{K_1}{L_\lambda}+1\right)} \qquad \text{Equation 5.3}$$

Where: *T* is the at-satellite temperature in Kelvin, K_2 is the calibration constant 2 (fixed at 1282.71 watts/metre2 *ster* µm for Landsat 7), K_1 is the calibration constant 1 (fixed at 666.09 watts/metre2 *ster* µm for Landsat 7) and $L\lambda$ is the spectral radiance in watts per metre squared. See the Landsat Science Users Handbook for more details Irish (1999).

Potential cloud pixels were identified using the exact thresholds set out in Irish (2000). An iterative process was used whereby; each ACCA filter threshold was used to create a region of interest (ROI), the ROIs were converted to binary masks and multiplied together with the binary masks from the other filters. "Pass two" filtering was not conducted as the images did not meet the three criteria mentioned above and in Irish (2000). Thus, the binary mask resulting from multiplying all ROI masks together was considered as the per-pixel cloud cover mask.

5.3.2. Adapting the Automated Cloud Cover Assessment Algorithm for Pixel Based Cloud Filtering in Assam

To standardise brightness differences between images acquired on different dates (Song et al. 2001) atmospheric correction was performed using ATCOR-2: Atmospheric Correction for Flat Terrain to remove medium level haze and convert the 30 m multispectral bands from all images to ground-based reflectance units (Richter 2007). The thermal band 6.1 was processed in exactly the same way as for the ACCA method in section 5.3.1.

Using ENVI 4.6 six of the eight "pass one" filters from the ACCA algorithm were applied to the data. Filter two and filter eight of the ACCA algorithm were excluded. The ACCA filter two is a normalized snow difference index (NSDI) (Irish 2000) and this was excluded as no snow was

present in the scenes once spatial sub-setting had removed the surrounding mountains. ACCA filter eight is a composite of ETM+ band 5 and thermal band 6.1 designed to separate identified clouds into hot and cold cloud categories and was excluded as splitting clouds by temperature was not required for this research. Cloud filter parameters offered the greatest discrimination between thick and transparent cloud and non-cloud when filter threshold values were varied for each image (Table 5.2).

Table 5.2 Thresholds used for the pixel based filtering of clouds

Image	ACCA filter 1	ACCA filter 3 (° K)	ACCA filter 4	ACCA filter 5	ACCA filter 6	ACCA filter 7	Additional filter A	Additional filter B
L7134_041	Cloud > 3.25	Cloud < 296	Cloud < -517	Cloud < 5	Cloud < 4.2	Cloud < 4.18	Cloud > 2.5	Cloud > 7.75
L7135_041	Cloud > 1.5	Cloud < 293.5	Cloud < - 60	Cloud < 10	Cloud < 2.7	Cloud > 1.5	Cloud > 1.75	
L7135_042	Cloud > 1	Cloud < 296.5	Cloud < -69	Cloud < 12	Cloud < 2.6	Cloud > 1.25		
L7136_041	Cloud > 0.75	Cloud < 296	Cloud < - 1100	Cloud < 13	Cloud < 3.7	Cloud > 0.99		
L7136_042	Cloud > 5.5	Cloud < 297	Cloud < 30	Cloud < 1.5	Cloud < 0.7	Cloud > 1.1		
L7137_041	*No Cloud*							

In scenes where cirrus cloud was present the thresholds for filters 1-6 had to be extended well past the normal cloud levels (Table 5.2). Therefore, to decrease the number of pixels identified as potential cloud two additional filters were developed (Table 5.2); i) Additional filter A and ii) additional filter B. Additional filter A used ETM+ band seven brightness levels to distinguish areas of transparent cloud from wet bare land and urban areas. Band seven brightness levels were used to distinguish areas of cirrus cloud from wet bare land or urban areas displaying similar spectral and temperature properties to clouds. Band seven was selected as it is in the mid infra-red region and thus less affected by atmospheric scattering. Thus it gave a clearer idea of areas that may have thin cirrus clouds. Additional filter B used Band two brightness levels to help further distinguish between areas of thin cirrus cloud and vegetation. Band two

presents clear differences between dark vegetation and brighter cloud pixels. The additional filters were employed in two images that had brighter overall pixel values due to increased levels of bare soil from agricultural harvests. All filter threshold parameters adapted from the ACCA algorithm and the two extended filters are presented in Table 5.2. Extending the ACCA thresholds was expected to decrease the omission errors relating to transparent clouds. However, it was also expected to introduce increased commission errors from pixels with similar properties to transparent clouds. Therefore, object-based analysis was used to reduce these errors by 'cleaning' the mask using spatial parameters to remove the pixels least likely to be clouds.

5.3.2.1 Object-based Analysis for cloud mask "cleaning"

The binary masks developed from spectral filtering described in Section 5.3.2 were input into eCognition Professional 5[15]. The multi-segmentation tool was used to create two levels of image objects (Darwish et al. 2003). Level-two segmentation had a scale factor of 10. The shape criteria is constructed of two parameters; i) compactness, which optimizes for the compactness of the resulting objects where a perfectly compact object is a square and, ii) smoothness, which optimises for the smoothness of object borders. The level-two segmentation had one class defined (potential cloud) and included all pixels with a value of one which were identified as potential cloud in the adapted pixel-based filters in section 5.3.2. The potential cloud class in level-two segmentation was used as the parent class for further analysis in level-one segmentation. Level-one segmentation was undertaken based on a scale factor of one. The homogeneity criteria included 95% emphasis on spectral homogeneity and 5% on shape. The shape parameter included 75% emphasis for compactness and 25% emphasis for smoothness. Within the level-one segmentation three child classes were created; large cloud, small cloud and non-cloud.

Using the level-two segmentation all objects with a value of one were classified as potential cloud and used as a parent class for subsequent analysis on the image from level-one segmentation. Objects from the level-one segmentation were classified as one of three child

[15] Definiens (2006) http://www.ecognition.com/products

classes; i) large cloud, ii) small cloud, iii) non-cloud. The objects were defined solely using spatial definitions as summarised in Table 5.3. The same three class descriptors were used for each image, but the spatial thresholds were optimized separately for each individual image as the size, thickness and brightness of clouds varied (Table 5.3).

Table 5.3 Class descriptions used for the object-based classification of clouds.

Cloud Mask Input	Level 2 Segmentation and Classification	Level 1 Segmentation and class descriptions		
	Potential Cloud	Large Cloud	Small Cloud	Non-Cloud
L7134_041	Object mean value = 1	Area > 50,000 m2	Area 7,500 – 50,000 m2 OR Distance to large cloud < 1000 m	Area <10,000 m2 AND Distance to large cloud > 1000 m2
L7135_041	Object mean value = 1	Area > 100,000 m2	Area > 5,000 – 100,000 m OR Distance to large cloud < 1000 m	Area < 5,000 m2 AND Distance to large cloud > 1000 m
L7135_042	Object mean value = 1	Area > 150,000 m2	Area 4,000 – 150,000 m2 OR Distance to large cloud < 1000 m2	Area < 4,000 m2 AND Distance to large cloud > 1000 m2
L7136_041	Object mean value = 1	Area > 30,000 m2	Area 900 – 30,000 m2 AND Distance to large cloud < 1000 m2	Area <30,000 m2 AND Distance to Large cloud > 1000 m2
L7136_042	Object mean value = 1	Area > 15,000 m2	Area 1,800 – 15,000 m2 OR Distance to Large Cloud < 1000 m2	Width < 60 metres
L7137_041			*No Cloud*	

5.3.3. Accuracy Assessment for cloud cover removal

An ROI equating to an approximate 10% sample of the total clouds from the object-based cloud filters was created for each image. Histogram stretching and visual interpretation was used to distinguish between transparent clouds and land covers. For each image an ROI of non-cloud pixels, approximately equal to the number of cloud pixels was also created. The resulting ROIs were used to create a sample image with three classes; cloud samples, non-cloud samples and remaining pixels. Error images were created by summing the sample image with the output masks from the ACCA filtering, the pixel-based filtering and object-based classification.

Confusion matrices and Cohen's Kappa coefficient (Congalton 1991; Foody 2002; Rosenfield and Fitzpatrick-Lins 1986) were calculated from the error images for each of the three methods and reported in error matrices. An error matrix allows the comparison on a category-by-category basis of the relationship between training data which are known and the predicted data resulting from the classification. The matrices highlight the errors of omission, where an object is selected as belonging to a class in the sample data but has been missed by the classification and errors of commission (where an object is classified as a different class to the one it is selected as in the sample data). The overall accuracy is calculated by dividing the total number of correctly classified pixels with the total number of pixels in the training data. Producer accuracy are defined as the number of pixels classified correctly in each class divided by the number of pixels used in the training data for that class. The producer accuracy shows how well the training data of a given class have been classified. The user accuracy is defined as the number of pixels classified correctly for each class divided by the total number of pixels classified in the category (Lillesand et al. 2004).

The Khat statistic results from calculating the Kappa Coefficient and it is a measure of the difference between the agreement between sample data and classified data and the chance agreement between the sample data and a random classifier (Lillesand et al. 2004). The Khat statistic for this research was calculated using Equation 5.4 which was taken from Congalton (1991) and Lillesand et al. (2004):

$$K_{hat} = \frac{N\sum_{I-1}^{r} x_{ii} - \sum_{i-1}^{r}(x_{i+} * x_{+i})}{N^2 - \sum_{i=1}^{r}(x_{i+} * x_{+i})}$$ Equation 5.4

Where: *r* is the number of rows in the error matrix; x_{ii} is the number of observations in row *i* and column *i* (on the major diagonal); x_{i+} is the total of observations in row *i* (marginal total to the right of the matrix); x_{+i} is the total observations in column *i* and *N* is the total number of observations included in the matrix. Thus, taking the object-based cloud classification image for WRS path/row 135/042 as an example, where the error matrix is shown in Table 5.4.

Table 5.4 Example error matrix for WRS path/row 135/042.

Image 5 Object-based Mask	Cloud	Non-cloud	Total
Cloud	38671	1	38672
Non-cloud	13379	51378	64757
Total	52050	51379	103429

From the error matrix for example image (WRS path/row 135/042) the Khat statistic was calculated using:

$$K = \frac{103429(38671 + 51378) - ((38672 * 52050) + (64757 * 51379))}{((103429\text{^}2) - ((38672 * 52050) + (64757 * 51379))}$$ Equation 5.5

Once the cloud cover had been identified and removed from each image and accuracy assessments conducted the cloud free imagery was then passed to the land cover classification procedure outlined below.

5.4. Land cover classification

Object-based land cover classification was conducted using eCognition Professional 5.5. Nine classes were identified, covering both land uses and land classes, based on knowledge from field work observations (Chapter 4) and relationships between census and environment

identified in the literature (Chapter 2). The classification procedure followed the guidelines for 30 m spatial resolution satellite sensor data set out in Anderson et al. (1976) and subsequently modified by the USGS for the United States National Land Cover dataset (Vogelmann et al. 2001; Jones et al. 2009) and used by Homer et al. (2004). Therefore, based on the above literature, the criteria followed for remote sensing classification included the following focus points:

- Minimum level of accuracy of 85%;
- Repeatable results needed;
- Applicable over extensive areas, and;
- Classification should allow land cover types to be used as a proxy for activities (land uses).

Classes identified were; bare, built up, grass, plantation, summer crop, water, wetland, winter crop and woodland. Landsat ETM+ images acquired prior to the main harvest time of October or November during the winter period during January were used to distinguish between winter crop and bare land.

Segmentation of the images produced homogeneous objects for classification using a scale parameter of 8 (which determines the size of the resulting objects). The homogeneity criteria included 90% emphasis on spectral homogeneity and 10% on shape (compactness and smoothness), and 50% for both compactness (optimises for the compactness of resulting objects; a perfectly compact object is a square) and smoothness (optimises for the smoothness of object borders). As recommended by Baatz et al. (2000) the segmentation criteria were based on experimentation with parameters to achieve objects with the desired size, homogeneity and shape for the application. The ETM+ band 1 in both the October and January data sets were weighted as zero in the segmentation process. Band 1 on the ETM+ sensor covers the blue portion of the electromagnetic spectrum and is subject to several problems relating to atmospheric contamination. Tasselled cap transformation wetness and greenness indices (Lillesand et al. 2004) were derived from October images in ENVI prior to segmentation

and used in the segmentation and classification process to assist in identifying wet pixels, and different types of vegetation. Bands two to five and seven of both the October and January images and the Tasselled cap wetness band were given a weighting value of one to ensure all were treated equally in the segmentation process. Each image was segmented using the same criteria. However, image WRS path/row 136/042 had to be split into two as the image was too large to be segmented and classified as one.

The classification procedure used for each of the land cover classes is detailed in Table 5.5. The nearest neighbour classifier was applied to six of the nine land cover classes and used a minimum membership of 0.5. Minimum membership was calculated using samples for each land cover class that were collected after segmentation. Spectral features used for nearest neighbour classification were, mean and standard deviation measures of the spectral values of bands two to five and seven in the October and January images and the mean and the standard deviation of the wetness and greenness bands from the Tasselled cap transformation for both October and January images. The customized features builder, in eCognition 5.5, was used to create Normalized Difference Vegetation Index (NDVI) for each object in both October and January images and these were used in the nearest neighbour definition along with the change in NDVI between October and January. Spatial features used in the nearest neighbour classifier included, object area, object length divided by object width, and object asymmetry.

Table 5.5 Class descriptions used for the object-based land cover classification.

Class	Definition	Image number
Bare	NN with samples	All
Grassland	NN with samples	All
Built Up	Manual	All
Summer crop	NN with samples	All
Winter crop	NN with samples	All
Water	Class description	All
Woodland	NN with samples	All
Wetland	Manual	All
Plantation	NN with samples. Area over specific threshold.	All

Areas of plantation in Assam are easy to identify visually through constant year round spatial and textural properties. Segmentation did not result in single plantation objects as they were spectrally very similar to the surrounding woodland and summer cropland. Therefore, prior to running the nearest neighbour classifier plantation objects were manually merged to form larger homogenous plantation objects. This meant that plantation could be identified using the samples and nearest neighbour classification with the addition of a class descriptor (minimum object size). The size of plantation objects varied for each Landsat image and the definitions used for each image are summarised in Table 5.6. The manual creation of large objects helped to distinguish plantation from other vegetation classes such as woodland that had small NDVI changes between October and January and similar spectral properties.

Table 5.6 Object area used to help classify plantation land.

Image Number	Area Threshold (square metres)
1 L134/041	> 500,000
2 135/041	> 500,000
3 135/042	> 500,000
4 136/041	> 500,000
5 136/042 Right	> 750,000
6 136/042 Left	> 750,000

In each image, a sample group of water was collected and summary statistics calculated which included:

- Mean October/November Band 5 and 7 value;
- Mean Tasselled Cap wetness, and;
- Mean NDVI for January.

These summary statistics provided a generalisation of water objects to be used to define the water class. Four class descriptors were used and these are presented in Table 5.7. Since class descriptors were used for water objects any object with water present was classified as

water. Wetland therefore had to be classified using manual editing instead of class descriptors or nearest neighbour classification.

Table 5.7 Object definitions used for classifying water

Image Number	Mean Oct B5	Mean Oct B7	Mean TC Wetness	NDVI Low
1	10 – 50	9 – 40	-15 - 33	-1 – 0.4
2	<9	0 – 5	-6 – 7	-1 – 0.5
3	<10	0 – 7	-6 – 20	-1 – 0.4
4	0 – 16.2	0 – 10.48	-9 - 20	-1 – 0.5
5 Right and Left	<12	0 – 10.48	-7.3 – 20	-1 – 0.4
6	0- 4.2	0 – 2	-0.15 – 20	-1 – 0.4

There were very few built up areas identifiable in the Landsat ETM+ imagery across the study region. Built-up areas had woodland, water, bare land and agricultural land within them which meant that the variance in the size and spectral properties of built-up objects were considerable. Thus, it was not possible to use nearest neighbour classification processes without having large numbers of bare land or shallow water objects wrongly classified as built up land. Therefore, built-up objects were manually classified once the nearest neighbour classification had been run.

GPS points representing specific land cover classes were collected during the field work and overlaid onto Google Earth imagery to identify how land cover classes looked in 2009. These classes were compared to Landsat imagery from 2001 to visually identify the land cover classes. Samples of these land cover classes were selected within the eCognition software to act as validation data for use in accuracy assessments. The areas where cloud had been masked were coded as no data and not used in the accuracy assessments.

5.4.1. Replacing the cloud removed objects with land cover data

Once the classification was complete all Landsat ETM+ images were mosaiced in ENVI 4.6 to form one raster data set for the study area. The ‘Expand’ function in the Spatial Analyst tool box

of ArcMap 9.3 was used to fill in the gaps left by the cloud removal procedure. The 'Expand' function expands selected values of a raster by a specified number of cells (ESRI 2009b). The pixels where cloud had been removed had values of zero and were specified as background zones, the nine land cover classes were specified as foreground zones. The 'Expand' function allows the foreground zones to expand into the background zones based on the value of the neighbouring cells. If there is more than one value that could be expanded into a background zone the function bases the expansion on the value of the majority of the surrounding cells.

5.5 Results

The results have been split into two sections (i) cloud cover removal and (ii) land cover classification. The full list of confusion matrices showing the differences between the ACCA mask and the extended ACCA mask are presented in Appendix 3a. Appendix 3b gives the full error matrices for the land cover classifications.

5.5.1 Cloud cover identification and removal

The confusion matrices (Appendix 3a) show increases in the numbers of cloud pixels identified from the ACCA mask to the pixel-based extended mask. As a result, the overall accuracies increased from 58.89% to 78.09%, 89.1% to 90.73%, 70.10% to 92.55%, 74.76% to 85.21%, 65.99% to 86.97% and 78.53 to 82.11% for images one to six respectively. Further, overall Kappa coefficients increased from 0.1625 to 0.5574, 0.7834 to 0.8156, 0.4066 to 0.8510, 0.4985 to 0.7043, 0.3203 to 0.7397 and 0.202 to 0.6531 for images one to six respectively. Error matrices are shown in Appendix 3a and total accuracy for the object-based cloud classification images are summarised in Table 5.8.

Table 5.8 Overall accuracy for each classified image using samples

Scene	Accuracy
L7134_041	82.12 %
L7135_041	94.55 %
L7135_042	94.94 %
L7136_041	88.87 %
L7136_042	87.06 %
L7137_041	86.69 %

The object-based classification procedure reduced the commission errors from the extended cloud mask by 5.47% and 8.72% in images three and four respectively. However, commission errors increased by 5.27%, 0.10% and 1.95% in images one, two and six respectively (Table 5.9). Manual editing was used to assign any unclassified objects to a class which reduced omission errors by 13.74%, 7.45% and 9.02% (Table 5.10) in images one, two and six respectively from the extended mask to the object-based mask. However, manual editing increased omission errors by 0.63%, 1.67% and 0.19% in images three, four and five respectively. Despite mixed results with regard to the omission and commission errors between the extended mask and the object-based mask, overall accuracies (Table 5.8) increased from 78.09% to 82.12%, 90.73% to 94.55%, 92.55% to 94.94%, 85.21% to 88.87%, 86.97% to 87.06% and 82.11% to 86.70% for images one to six respectively. Kappa coefficients increased from 0.5574 to 0.6403, 0.8156 to 0.8913, 0.8510 to 0.8988, 0.7043 to 0.7779, 0.7397 to 0.7417 and 0.6531 to 0.736 for images one to six respectively.

Table 5.9 Commission errors for the cloud removal techniques

	ACCA Filter	Extended Filter	Object-based mask
Image 1	0%	0.38%	5.65%
Image 2	0.04%	0.38%	0.48%
Image 3	0%	9.16%	3.69%
Image 4	0.05%	12.40%	3.26%
Image 5	28.49%	0.4%	0.0%
Image 6	5.6%	0.09%	2.04%

Table 5.10 Omission errors for the cloud removal techniques

	ACCA Filter	Extended Filter	Object-based mask
Image 1	84.04%	44.40%	30.66%
Image 2	20.97%	17.50%	10.05%
Image 3	59.03%	5.77%	6.40%
Image 4	49.75%	17.11%	18.78%
Image 5	39.46%	25.51%	25.7%
Image 6	32.25%	29.99%	20.97%

On average the percentage decrease in omission errors from ACCA filter to object-based masking was 35.08% and can be visualised in Figure 5.1 where the ACCA mask failed to identify the transparent parts of clouds. Image three, four and six had slight increases in omission errors from the extended mask to the object-based mask which was expected and is discussed in section 5.6. As expected commission errors increased from negligible values in the ACCA masks to larger values in the object-based mask (Table 5.9). However, object-based mask reduced commission errors from that of the extended mask in two images.

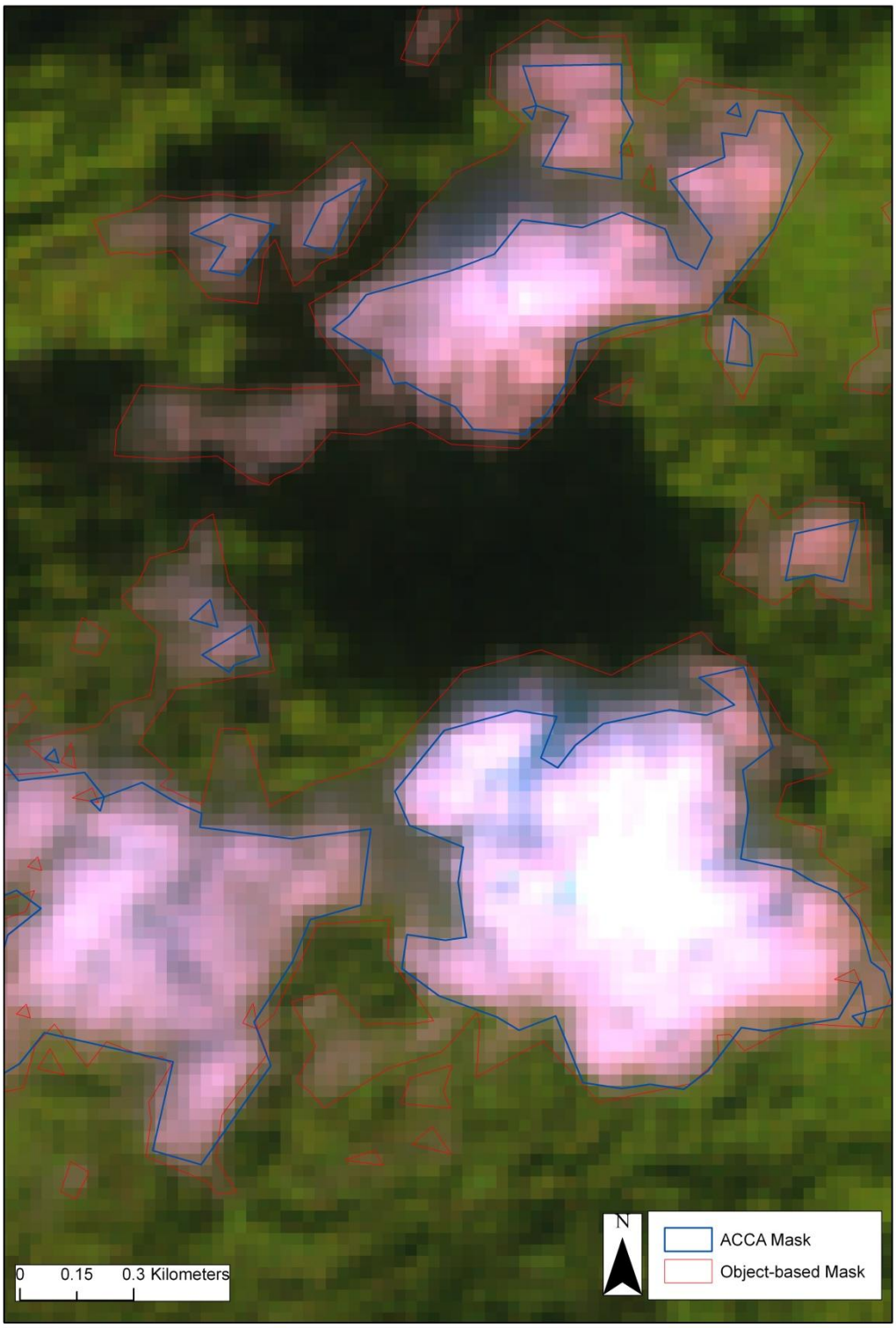

Figure 5.1 Outline of the cloud identified by the ACCA mask (blue) and that identified by the object-based mask (red) overlaid onto an RGB false colour composite of Landsat ETM+.

Image one was problematic for all cloud masking methods all cloud masking methods had higher omission levels for this image. This may be related to the lack of clouds in the image with just 0.19% reported in the image metadata. Images are classified as cloud free if the

ACCA filter reveals that less than 0.4% of the image is covered in cold cloud (Irish 2000). The majority of visible clouds were small transparent clouds which is probably why the ACCA filter reported such low cloud coverage. The clouds were difficult to identify computationally or visually against the relatively bright background due to a large amount of bare agricultural land, sand bars and banks and lower amounts of dense forest and vegetation.

Overall accuracy and Cohen's Kappa coefficients increased significantly for all four images from the ACCA mask to the object-based masks (Table 5.4). There were significant increases in overall accuracies and Kappa coefficients between the basic ACCA mask and the extended mask before object-based mask for images one, three and four. More modest increases in overall accuracy were seen between the extended thresholds mask and the object-based mask. However, in all four images there were large increases in the Kappa coefficients between the extended filter mask and object-based mask.

5.5.2 Land cover classification

The error matrices for all classified images can be found in Appendix 3b and the overall accuracy percentages for each image are summarised in Table 5.11. Overall accuracy ranged from 93.61% for image 135/041 (WRS Path/Row) to 98.62% for image 137/041 (WRS path/row) which are all above the 85% threshold advised by Anderson et al. (1976).

Table 5.11 Overall accuracy for each Land cover classification

Scene WRS Path/Row	Accuracy
134/041	95.82
135/041	93.61
135/042	98
136/041	96.37
136/042_Left	97.14
136/042_Right	97.05
137/041	98.62

Figure 5.2 shows the land cover classification for the entire research area in Assam. Figure 5.3 is a zoomed in image of part of the land cover classification where cloud was replaced with land cover data from the surrounding area using the expand function in ArcMap 9.3. On the whole the expand function appeared to work satisfactorily. No analysis was conducted on the accuracy of the expand method but it can be seen that when there are few land cover classes the resulting imagery appeared adequate.

Omission and commission errors were low for all classes apart from wetland and plantation. There was some omission of wetland objects and woodland, summer cropland and water. The wetland objects often fringed areas of water and were initially classified as water from the class descriptors. The manual editing phase then re-classified those objects that were felt to be wetland. Thus, there was large scope for human error in missing wetland objects. Furthermore, wetland also had similar spectral and spatial properties to woodland objects either under cloud shadow or within steep valleys. Very wet summer cropland also had similar properties to wetland objects. This meant that manually classifying wetland was expected to be limited.

The confusion between plantation and woodland was consigned to areas where woodland infringed on plantation and had large objects from the segmentation or where plantation objects had been missed when manually merging objects. This resulted in plantation objects not meeting the minimum object size criteria and instead being classified as woodland as the spectral properties were similar.

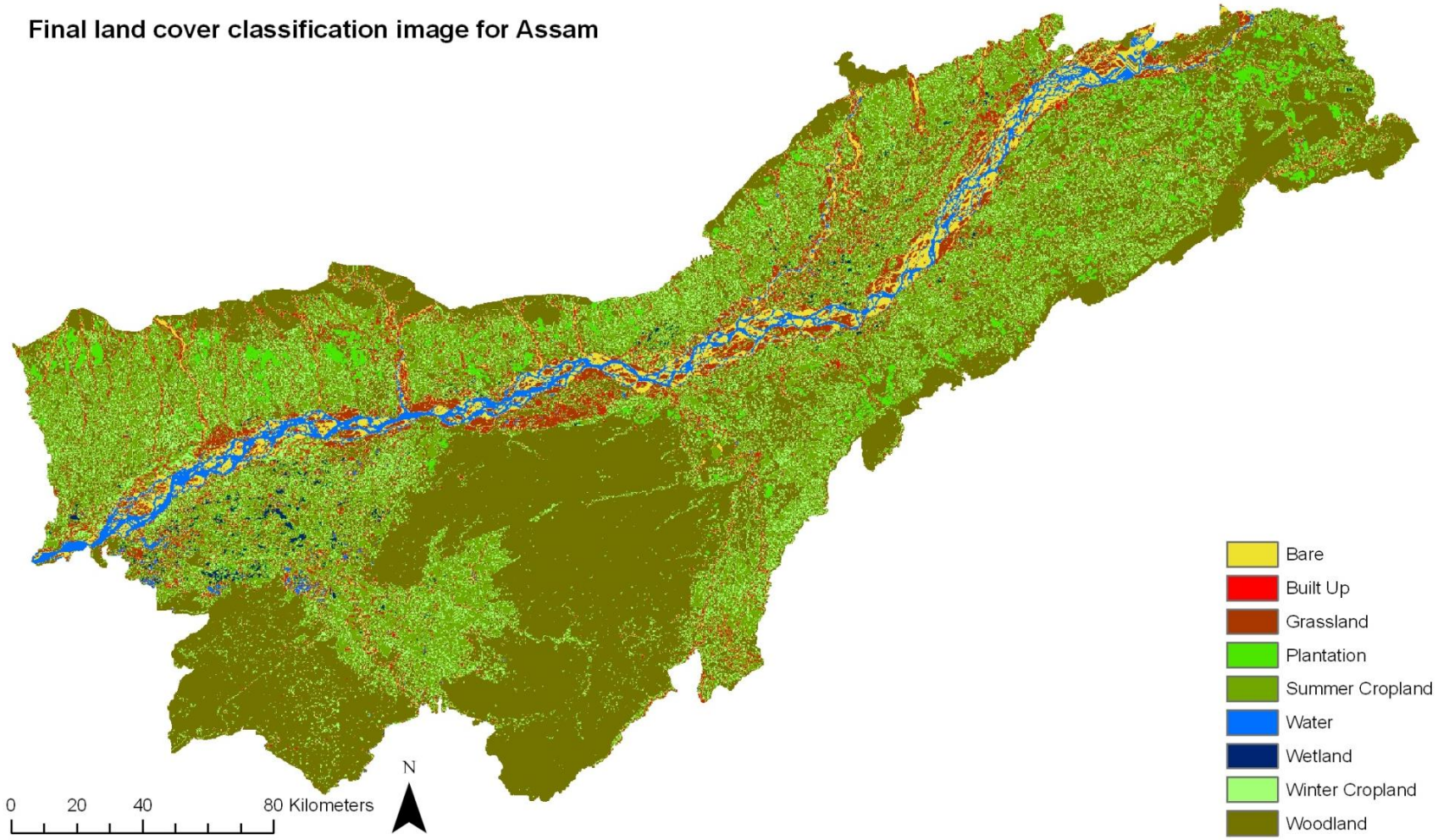

Figure 5.2 Land cover classification map for study area.

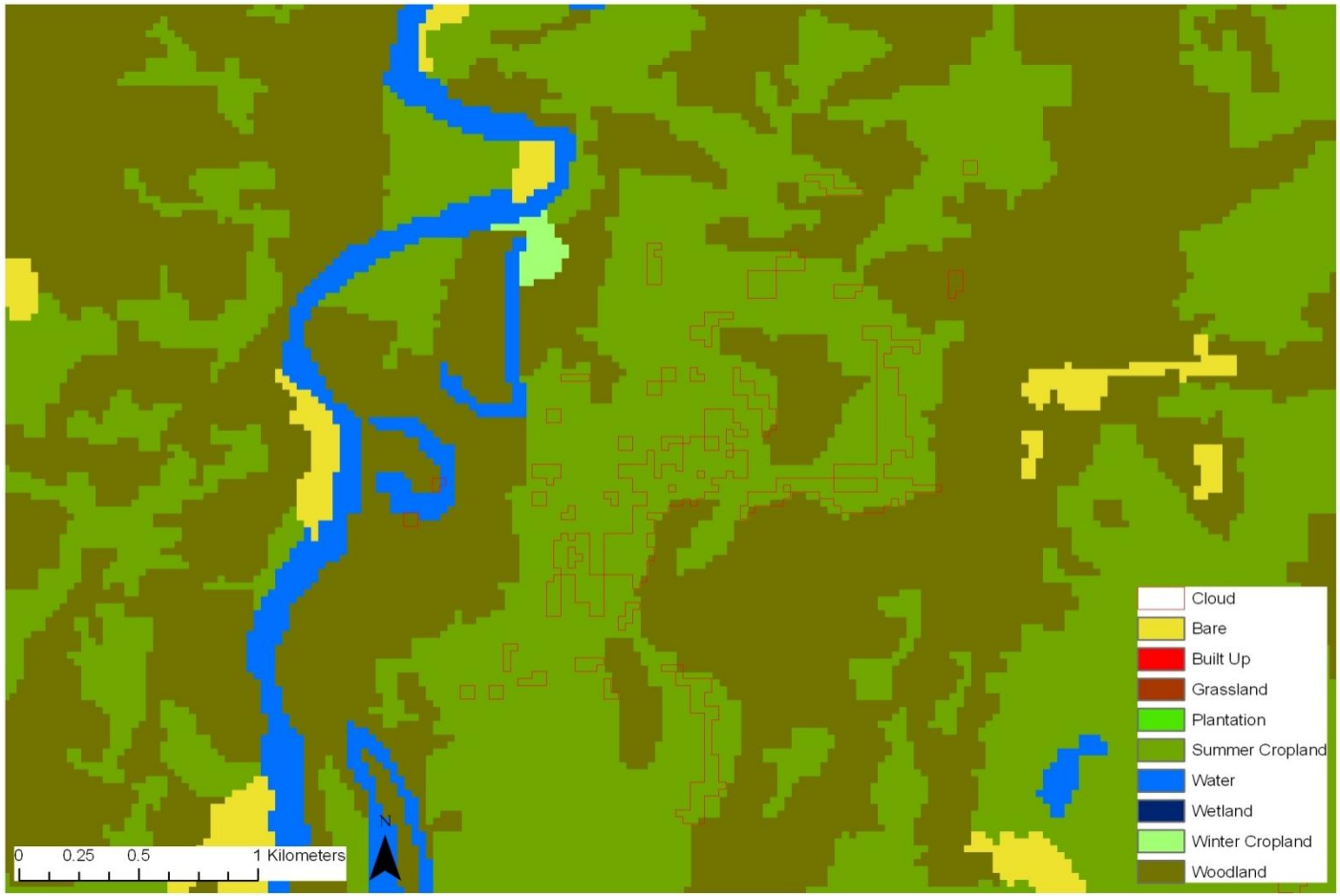

Figure 5.3 the effect of the 'expand' function for expanding surrounding land into the areas of cloud (outlined in red).

5.6 Discussion

Overall land cover classification procedure was able to provide nine land cover classes that were deemed important for subsequent statistical analysis with census variables and is discussed in greater detail in Section 5.6.2. The cloud cover identification and removal appeared to provide more accurate masking of transparent clouds and this is discussed further in Section 5.6.1.

5.6.1 Cloud cover identification and removal

The image-based technique to remove transparent clouds from individual images developed here used existing tool sets in widely available software packages. Kappa coefficients and overall accuracies increased for all images from the ACCA mask to the object-based mask. Overall accuracies for five of the six images were above the 85% threshold stated by Anderson et al. (1976). Omission errors were reduced substantially from the ACCA mask to the object-based mask for all images. Although, as expected, commission errors increased slightly from almost zero in the ACCA masks to between 0.5% and 5.65% in the object-based mask.

Omission and commission errors are important considerations for operational methods as they can lead to inaccuracies in the subsequent use of imagery for land cover classifications. Omission errors in images three, four and five were found to increase slightly from the extended mask to the object-based mask. This is a result of the definitions used in object-based classification. If small clouds existed in the imagery and were over a specific distance away from large clouds they would have been classified as non-cloud. These slight increases in omission errors were countered by much larger decreases in commission errors in both images.

Altering the ACCA filters can increase the commission errors in binary cloud masks. In an operational setting this may decrease the number of pixels available for land cover classifications. The object-based classification of cloud masks was designed to avoid masking large areas of non-cloud. Figure 5.4 show that it was relatively accurate in removing non-cloud objects whilst maintaining the majority of cloud objects. Commission errors increased

significantly in image one possibly due to brighter background pixels leading to erroneous classification of non-cloud objects during manual editing.

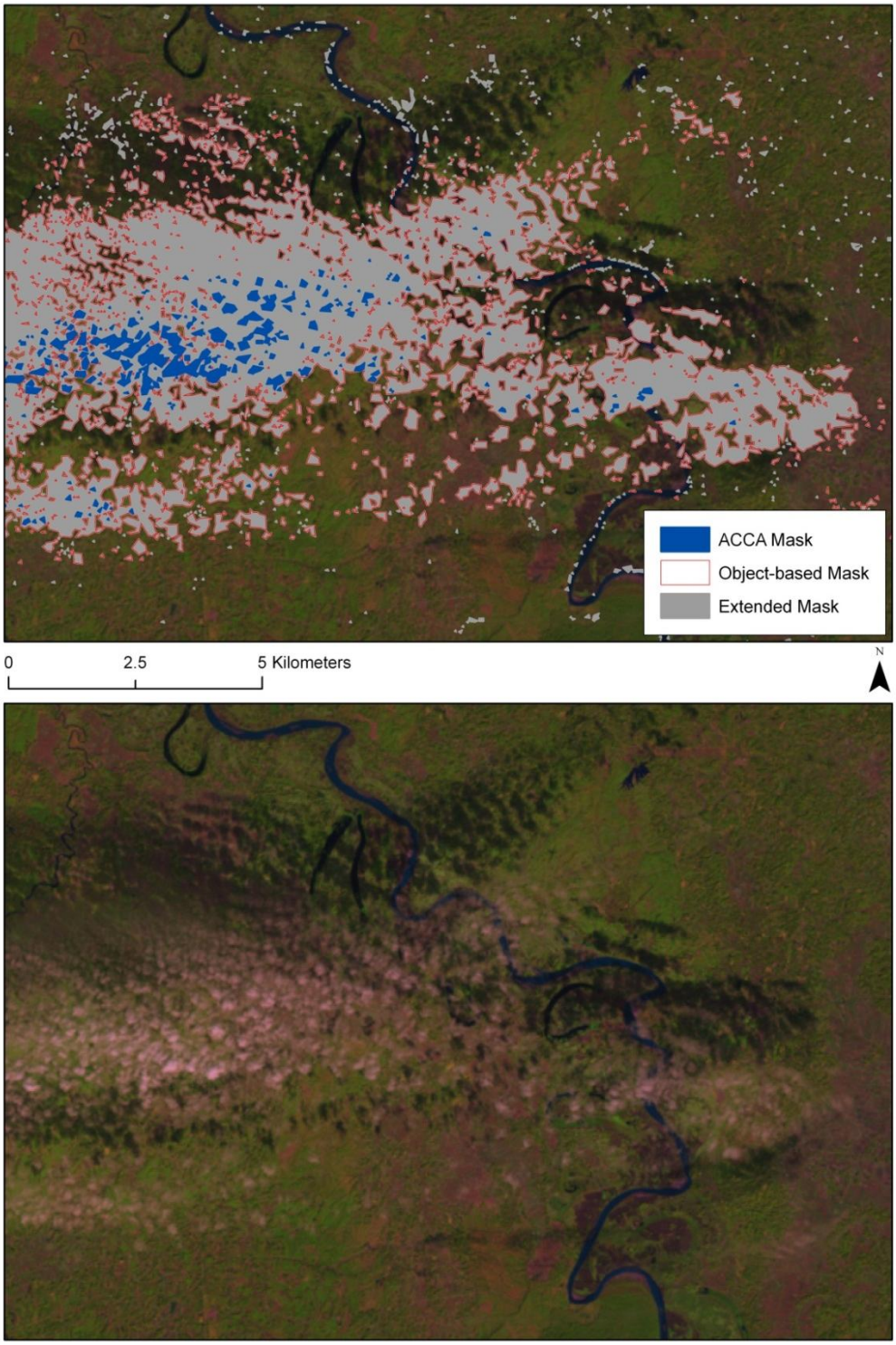

Figure 5.4 The object-based classification "cleaning" process. The extended cloud mask resulted in large amounts of commission errors. Using the object-based mask removed large amounts of non-cloud pixels from the mask. Grey coloured objects with a red outline were classified as cloud and those with no outline classified as non-cloud.

Problems may occur if ACCA filter thresholds are extended too far. The cloud cover mask may incur increased commission errors. If non-cloud pixels are adjacent to one another they will result in larger objects being created during object-based image segmentation. This will make it more difficult to distinguish between cloud and non-cloud using the current spatial class definitions. Therefore, future research may focus on performing object-based classifications on the multispectral imagery and using spectral and spatial definitions rather than using spatial definitions on a binary mask.

5.6.1.2. Limitations of the cloud cover identification and removal method

Prior to analysis it was hoped that one set of threshold extensions and object-based definitions would be sufficient to identify and remove transparent clouds from all five images. Histogram matching was attempted in ENVI mosaic tools prior to analysis. However, the spectral responses for specific land covers were not uniform, possibly due to the different dates of images and the time of year of acquisition coinciding with the start of rice harvests. The failure of histogram matching may be explained by Wen et al. (2001) who found that clouds and distance to clouds can lead to under predictions of surface reflectance. Therefore, differences in illumination between scenes remained and thresholds had to be adapted for individual images. This image-specific approach is not ideal, as it is more difficult to fully automate. However, the method was developed on a pragmatic basis in an operational environment that required specific images to be used in subsequent research. Accuracy assessment results show that it offered significant increases in accuracy in identifying and masking cloud and visible transparent clouds.

It was difficult to assess fully the accuracy of methods to identify transparent cloud. Image enhancement tools available in the software were used to help distinguish between transparent cloud and underlying land. However, any optically thin clouds in the scene that cannot be seen by the user are likely to have been left unmasked. This cannot be avoided as it is related to the spectral resolution of the Landsat ETM+ sensor. However, sharpening the multispectral imagery using the panchromatic band may help to further enhance the identification of cloud edges (Irish et al. 2006).

Image fusion techniques similar to those used by Helmer and Reufenacht (2005) to replace the masked areas with the correct land cover information were not attempted here. Extensive cloud coverage related to the monsoon meant a lack of available scenes immediately before those used, and images immediately after those acquired in October had very different spectral properties due to the harvest. Therefore, errors were likely in fusion techniques from differences in agricultural vegetation seasons which affect vegetation and soil phenology.

Future research could integrate shadow removal into the technique applied here by using geometric relationships between clouds and their shadows and brightness values as described in Martinuzzi et al. (2007). Further, a comparative study could compare the accuracies of the method developed here with other cloud masking methods highlighted in Section 5.2 to identify the most comprehensive cloud identification technique (although results may vary depending on the local conditions in the images used).

5.6.2 Land cover classification

The spatial and spectral parameters used in the nearest neighbour classifier were the same for all the images but the parameter thresholds were varied. The class descriptors used to define water and to support the nearest neighbour classifier of plantation were varied in each image to ensure greater accuracy. This approach was time consuming and would be problematic for extensive areas of research (Pax-Lenney et al. 2001) as the methods were not entirely repeatable or applicable over extensive areas (Anderson et al. 1976). However, this method ensured that the differing spectral and spatial parameters inherent in the images did not cause increased errors to result from generalising the classification process.

Creating an image stack for the classification which incorporated images from two distinct time periods during the agricultural calendar with NDVI and Tasselled Cap Transformation products meant that it was possible to distinguish between classes that would otherwise have been classified as a single land cover. For example, in the October/November images winter crop often lacked any vegetation cover. Thus, it had very similar spectral characteristics with bare land. Adding in images from January increased the distinction between winter cropland and

bare land classes through the use of spectral change detection in the multispectral bands and NDVI images.

A problem using images from two distinct time periods in an area affected by monsoon rain were the very large differences between the amounts of water in the river channels in October compared to January. Segmenting the images using the TC wetness band derived from the October image and not January meant that the extent of the water could be used to define the object boundaries. However, this means that the water class is only representative during October and may not have any similarity with the amount of water present at other times of the year.

No differences in spatial or spectral parameters could be found between the woodland and plantation classes. Thus, the manual object merge tool had to be used to increase the size of the plantation objects, which were very distinct visually from other classes. Some woodland objects were larger than the minimum plantation object area and therefore these errors had to be rectified using the manual editing tool.

5.6.2.1. Limitations of land cover classification

The 30 m spatial resolution of Landsat ETM+ data meant roads could not be identified in the classification. Pan-sharpening tools could be used in the future to create a data set with an effective spatial resolution of 15 m which may enable some of the larger roads within Assam to be detected by an automated classification process. A further problem resulting from the spatial resolution of Landsat ETM+ was that small ad-hoc agricultural areas on river banks and island could have been missed due to average field sizes often being lower than 30 by 30 metres.

Small settlements cannot be identified using 30 m resolution imagery. Henderson and Xia (1997) discussed the use of Synthetic Aperture Radar (SAR) for identifying human settlements and Tatem et al. (2004) found that "*...the combination of medium spatial resolution multispectral satellite imagery [Landsat TM] with similar scale SAR imagery and derived texture layer [was] effective in identifying and mapping settlements at medium-scale resolution across the diverse*

landscapes of Kenya" (Tatem et al. 2004, p.49). This may be a method to explore further in the future as it could add provide vital information relating to the location of human settlements.

The accuracy assessment conducted for land cover classification relied upon samples selected from within the images. Some of the images had very few objects belonging to the plantation, wetland or built up classes. Therefore, the number of samples available was often low which could potentially distort the overall accuracy estimates. A more detailed accuracy assessment would require the collection of ground data from around the time of the satellite data acquisition which was not possible here due to the use of historical data.

The winter cropland class was identified as an important environmental parameter during field observations. However, the number of crops harvested per year is much more complicated than just summer and a winter crop in Assam. Crops are planted depending on the rainfall and when rainfall is late this can delay the planting of the second crop (termed winter cropland in this research). This means that there is a strong likelihood that only using images from two periods during the agricultural calendar may result in some areas that grow second or third crops being missed.

The 'Expand' function was used as an efficient way of replacing land that was masked by cloud. In the future image compositing or geostatistical methods such as Kriging could be used to identify the most likely land cover under a cloud. However, problems may be encountered if substantial land cover changes occur between composited images, such as large scale flooding or land erosion, or if substantial cloud cover persists.

5.7 Conclusion

The ACCA algorithm was designed to provide fast automated assessments of cloud cover in Landsat ETM+ images to aid wider USGS mission aims for data acquisition. This research suggests that the ACCA method can be used in operational settings as the basis for a supervised step-by-step approach to extend the thresholds to identify and mask transparent cloud pixels. Object-based analysis principles can then be used to minimise the inevitable

commission errors emanating from visually extending the thresholds, thus, preserving more pixels for subsequent analysis and reducing potential inaccuracies in future land cover classifications.

Initial research attempted to find optimised filter threshold ranges that included transparent clouds in all images. However, it was found that cloud properties varied in each image. Therefore, filter threshold parameters for individual images were altered to ensure the highest possible overall accuracy for identification of thick cloud and transparent cloud whilst minimising commission errors.

Overall, omission errors were much smaller in the object-based mask than the ACCA mask meaning that subsequent land cover classifications will be more reliable with less inaccuracies associated with cloud that has been inadvertently excluded from the mask. Commission levels increased slightly from the ACCA filter to the 'cleaned' mask. However, the process of extending the ACCA filters, which were optimised using global data sets, is expected to include increased numbers of non-clouds. The object-based classification helped to reduce commission errors in two of the four images and there was little change in a third image.

The adapted cloud cover identification and masking procedure produced a set of images for land cover classification with greater reduced amounts of cloud within them. This meant that it was easier to identify and classify land cover classes accurately that were thought to have important associations with poverty and development. Had the cloud removal procedure not been conducted certain land cover classes with spectral and spatial properties similar to transparent cloud would have been less accurate. These inaccuracies may have had the effect of causing bias into the subsequent statistical analyses as there would have been increased amounts of bare land within the database that was not actually bare land.

Overall, the cloud cover removal algorithms provided a database in which to derive environmental metrics for subsequent analysis more accurately which would also then lead to increased confidence in the subsequent statistical analysis results.